

A Highly Active and Support-Free Oxygen Reduction Catalyst Prepared from Ultrahigh-Surface-Area Porous Polyporphyrin**

Shengwen Yuan, Jiang-Lan Shui, Lauren Grabstanowicz, Chen Chen, Sean Commet, Briana Reprogle, Tao Xu, Luping Yu,* and Di-Jia Liu*

A new approach for preparing non-precious-metal electrocatalysts using a porous organic polymer (POP) as precursor is presented. Polyporphyrin, containing a high density of nitrogen-coordinated iron macrocyclic centers, was prepared by oxidative coupling to form a porous network with a very high specific surface area and narrow pore-size distribution. Upon pyrolysis, the POP was converted into a highly active electrocatalysts for the oxygen reduction reaction in an acidic electrolyte. Proton-exchange membrane fuel cells, prepared with such catalyst at the cathode, achieved very high measured volumetric and gravimetric current densities of 20.2 A cm^{-3} and 39.4 A g^{-1} at 0.8 V, respectively, and a peak power density of 730 mW cm^{-2} at 0.4 V.

The proton-exchange membrane fuel cell (PEMFC) is among the most efficient energy conversion devices for future transportation applications.^[1] The PEMFC is operated through the electrochemical hydrogen oxidation reaction (HOR) at the anode and oxygen reduction reaction (ORR) at the cathode. The ORR generally faces higher kinetic barrier than HOR and therefore requires more catalyst.^[2] At present, the electrocatalysts of choice are precious metals, such as platinum supported on a carbon substrate. High costs and limited reserves of the precious metals pose a major challenge for large scale commercialization of PEMFCs.^[3] Non-precious-metal catalysts (NPMCs) made of Fe and Co in carbon composites have attracted a great deal of attentions since they were discovered with promising activities towards ORR in

acidic media.^[4] Their activities in alkaline or neutral media were also extensively studied, although the subject is beyond the scope of the current discussion.^[5] Extensive characterizations have been carried out in attempts to understand the roles of transition metals, nitrogen, and surface properties in the catalytic activity of these NPMCs.^[6] The durability of these NPMCs in the protonic medium has been a major concern, although recent work by Wu et al. demonstrated a catalyst with improved stability in the PEMFC operating environment.^[4i] At present, the catalytic activities of NPMCs are still significantly less than that of precious metals. To make NPMCs truly competitive, substantial improvements in two critical properties have to be accomplished: 1) a higher turnover frequency (TOF) per active site; and 2) a greater catalytic site density per unit volume. To improve TOF requires an in-depth understanding of the influences by transition metals, organic ligands, and the support on the active site. The interdependences between these factors are still under intensive investigation.^[4i] To improve active site density, a NPMC precursor with densely populated metal–ligand sites and high surface exposure, and preferably free of inactive support, such as carbon, would be a rational starting point. For example, the volumetric current density of NPMCs prepared by impregnating transition metal salt over porous carbon appeared to have reached an upper limit, although performances were recently elevated through pore filler and pore former approaches.^[4h,7] More recently, NPMCs prepared using the metal–organic frameworks (MOFs) as precursors have generated excellent catalytic performances.^[8] In MOFs, the frameworks are built through the metal–ligand interaction with well-defined coordination chemistry and the highest possible precursor site density.^[8a] One key issue with MOF-based NPMC preparation is the removal of the high level of metal, which is currently accomplished by either high-temperature vaporization during the thermolysis^[8b] or an acid wash after heat treatment.^[8c] In either approach, limitations on the experimental conditions affected the versatility of the method.


Herein we describe a new approach of preparing highly active NPMCs using porous organic polymer (POP) precursors containing densely populated transition-metal–nitrogen coordination sites uniformly decorated over the micropore surface. POPs have recently emerged as a new class of gas-storage and separation materials.^[9] A broad selection of monomers and cross-linking reactions provide great flexibility for producing very-high-surface-area POPs containing different functional groups. When nitrogen-containing macrocyclic functional groups, such as porphyrin or phthalocyanine, are employed as the oligomers for the synthesis, the new

[*] Dr. S. Yuan,^[†] Dr. J. Shui,^[†] C. Chen, S. Commet, B. Reprogle, Dr. D.-J. Liu
Chemical Sciences & Engineering Division
Argonne National Laboratory, Argonne, IL 60439 (USA)
E-mail: djliu@anl.gov

L. Grabstanowicz, Prof. Dr. T. Xu
Department of Chemistry and Biochemistry
Northern Illinois University, DeKalb, IL 60115 (USA)
Prof. Dr. L. Yu
Department of Chemistry and The James Franck Institute
The University of Chicago, Chicago, IL 60637 (USA)

[†] These authors contributed equally to this work.

[**] This work was supported by the U.S. Department of Energy's the Office of Science and the Office of Energy Efficiency and Renewable Energy Fuel Cell Technologies program. The authors are grateful to Dr. Jiangbin Xia, Dr. Jun Lu, Dr. Deborah J. Myers, and Alex Mason for their support with experiments.

 Supporting information for this article, including details of PFETTPP catalyst and MEA preparations, RRDE and single cell tests, catalyst durability studies, and surface-material property characterizations, is available on the WWW under <http://dx.doi.org/10.1002/anie.201302924>.

POPs could incorporate a very high density of metal–N₄ ligation sites evenly distributed inside of the porous network.^[9c] A transition-metal–N₄ macrocyclic compound was the very first candidate for a NPMC electrocatalyst.^[10] Improved catalytic activity, using thermally activated porphyrins, was continually reported until recently.^[4e,p] Herein, we demonstrate the design and preparation of a new NPMC using a POP with an ultrahigh surface area and a high density of iron–porphyrin groups. The new catalyst was evaluated in the acidic electrolyte using a rotating-disk electrode method and in PEMFC test. Excellent ORR catalytic activity and fuel-cell performance were found.

Syntheses of polymerized 5,10,15,20-tetrakis-(3,5-di-thiophen-2-yl-phenyl)porphyrin (PTTTP) and its iron-metallated version PFeTTPP, where Fe²⁺ was coordinated by a porphyrin ring, have been reported previously by our team.^[9c] Figure 1 shows a simplified synthesis and the molecular and the three-dimensional stacking structures of PFeTTPP. Elemental analysis indicated that about 2.1 wt % of Fe was retained in PFeTTPP, suggesting that about 50 % of the porphyrin rings were coordinated with iron(II) ions. From the packing density and molecular weight, the number of macrocyclic Fe/N₄ sites per unit volume and weight of the as-synthesized PFeTTPP was calculated to be $1.56 \times 10^{20} \text{ cm}^{-3}$ and $4.68 \times 10^{20} \text{ g}^{-1}$, respectively.

The PFeTTPP powder was thermally activated under flowing nitrogen without any additional treatment. The samples were pyrolyzed from 600 to 1000 °C and labeled by their activation temperatures. For example, PFeTTPP-700 indicates the activation temperature of 700 °C. The activation duration was controlled at one hour. The ORR electrocatalytic activity of the sample after thermolysis was first studied using a rotating ring-disk electrode (RRDE) method in an oxygen saturated HClO₄ acid solution. Although as-synthesized PFeTTPP showed little catalytic activity, it started to become active towards ORR after being pyrolyzed at 600 °C (Figure 2a) as the organic species was in the process of being converted into carbon. The activity increased dramatically when the temperature reached to 700 °C (PFeTTPP-700) with an onset potential (E_0 , measured at mass activity of 0.02 A g^{-1}) of 0.93 V and a half-wave potential ($E_{1/2}$) of 0.73 V, all were measured in reference to the reversible hydrogen electrode (RHE). Interest-

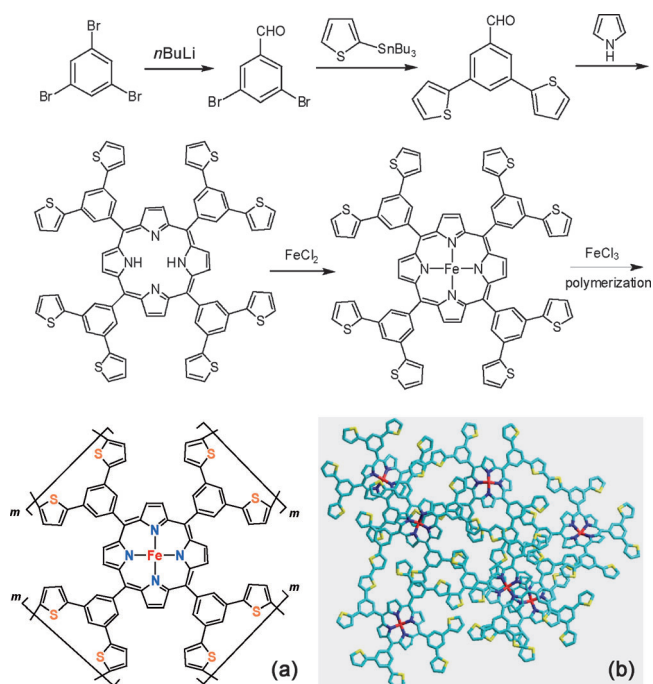


Figure 1. Synthesis of PFeTTPP. a) Molecular structure; b) simulated 3D stacking of PFeTTPP. Fe red, N blue, C light blue, S yellow; H not shown for clarity.

ingly, further increase of the thermolysis temperature to 800 °C (PFeTTPP-800), 900 °C (PFeTTPP-900), and 1000 °C

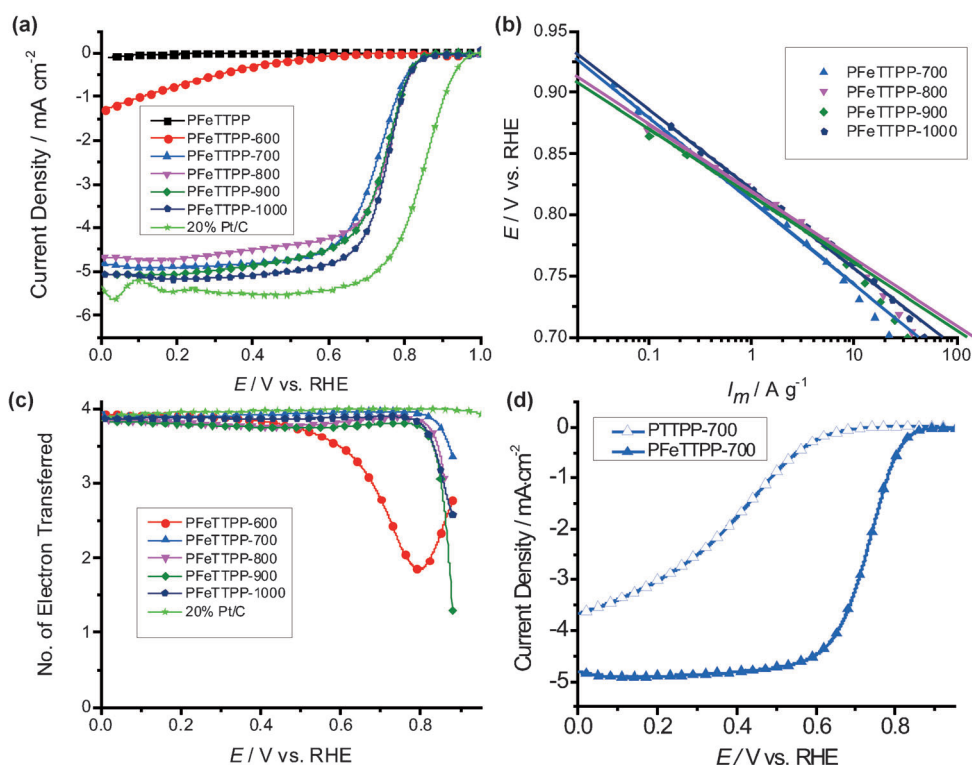


Figure 2. RRDE measurements of a) polarization currents of PFeTTPP samples activated at different temperatures; b) Tafel plots; c) number of electron transferred; and d) activity comparison between 700 °C activated Fe-free and Fe-containing polyporphyrins. Condition: O₂-saturated HClO₄ solution (0.1 M) at 1600 r.p.m. and 20 °C; catalyst loading = 0.4 mg cm^{-2} . For comparison, Pt/C data also provided in (a) and (c).

(PFeTTPP-1000) only altered the catalytic performance slightly. This observation is in fact strikingly different from the earlier studies on MOF-based catalyst precursors, where the optimal temperature was sensitive to the precursor composition (700 to 800 °C for Co or Fe zeolitic imidazolate framework or 1000 °C for ZIF-8).^[8] The structural and chemical changes of the pyrolyzed PFeTTPP will be discussed below and in the Supporting Information; the results of RRDE measurement are summarized in Table 1.

Table 1: Electrocatalytic performance of PFeTTPP activated at different temperatures.

Sample ^[a]	<i>T</i> ^[b] [°C]	<i>E</i> ₀ ^[c] [V]	<i>E</i> _{1/2} [V]	<i>N</i> _e ^[d]
PFeTTPP-700	700	0.93	0.73	3.96
PFeTTPP-800	800	0.91	0.75	3.84
PFeTTPP-900	900	0.91	0.75	3.64
PFeTTPP-1000	1000	0.93	0.76	3.80
PTTPP-700	700	0.73	N/A	N/A

[a] All of the RRDE data were measured in O₂-saturated HClO₄ solution (0.1 M) at 20 °C. [b] Thermolysis temperature (*T*). [c] Measured at a mass activity of 0.02 A g⁻¹. [d] Measured at 0.8 V.

Figure 2b shows the Tafel plots of mass activities (*I*_m) for the PFeTTPP samples activated from 700 to 1000 °C calculated using the following Equation (1):

$$I_m = \frac{-I_k}{m_{\text{cat}}} \quad (1)$$

where *I*_k is the kinetic current and *m*_{cat} is the mass of the catalyst.^[4p] These Tafel plots are nearly overlapped with each other between 0.7 to 0.9 volts with the slopes differing slightly from 55 to 67 mV/decade. The RRDE experiment also enabled the measurement of the electron transfer number *N*_e at different ORR potentials during the polarization. Figure 2c shows the electron-transfer number as the function of the potential. All of the *N*_e values were nearly four for the potential between 0 and 0.8 V, suggesting a dominant four-electron process of converting oxygen to water, a preferred mechanism for hydrogen fuel cells. The *N*_e values measured at 0.8 V are also listed in Table 1. The *N*_e values can also be used to calculate the hydrogen peroxide generated at different polarization potential (see the Supporting Information). We found that H₂O₂ production was fairly low for PFeTTPP thermally activated over 700 °C. For example, less than 2 % H₂O₂ was generated in a wide potential range up to 0.8 V. A commercial 20 % Pt/C sample was also investigated and included in Figure 2 for comparison.

To understand the influence of the transition metal on the active site formation, we also heat-treated an iron-free polyporphyrin, PTTPP, at 700 °C for 1 hour (PTTPP-700). The RRDE measurements of PTTPP-700 and its iron-containing counterpart, PFeTTPP-700, are shown in Figure 2d. A clear distinction was found between the two. For PTTPP-700, an onset potential of only 0.73 V was observed and no limiting current was attained. In contrast, PFeTTPP-700 showed a much higher activity and O₂ was mostly reduced

to H₂O by a four-electron mechanism (see the Supporting Information).

The catalytic activity of the heat-treated PFeTTPP was also investigated by single-cell tests. The catalysts were fabricated into the Nafion membrane electrode assemblies (MEAs) and evaluated under PEMFC operating condition using fully humidified oxygen at the cathode and hydrogen at the anode. Figure 3a shows the Tafel plot in both gravimetric

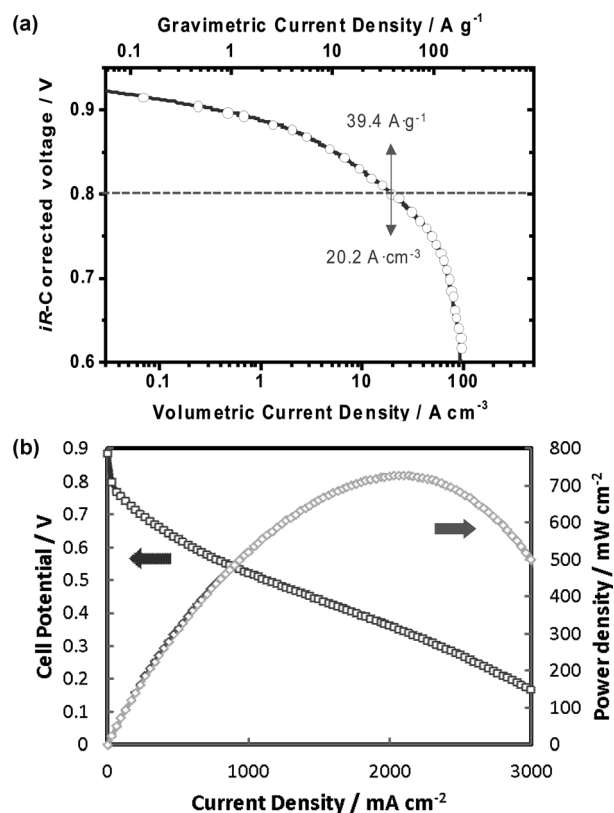


Figure 3. a) Tafel plot of a MEA in single cell test, membrane = Nafion 117, cathode catalyst PFeTTPP-700 at 4.0 mg cm⁻², anode catalyst Pt/C at 0.25 mgPt cm⁻², cell area 5 cm², *T* = 80 °C, *p*_{O₂} = *p*_{H₂} = 1 bar (converted), flow rates at 300 mL min⁻¹; b) The current-voltage polarization and power density from another single-cell test, Nafion 211 membrane, cathode catalyst PFeTTPP-1000 at 4.1 mg cm⁻², anode catalyst Pt/C at 0.3 mgPt cm⁻², cell area 2 cm², *p*_{O₂} = *p*_{H₂} = 1.5 bar, other conditions were the same as (a).

and volumetric current density scales obtained from a current-voltage polarization study (Supporting Information, Figure S2). The MEA was prepared using Nafion 117 to reduce the cross-over current for a more accurate catalytic activity measurement. The plot was derived after converting O₂ and H₂ pressures to 1 bar.^[4j] The volumetric current density was calculated based on the actual cathode catalyst layer thickness measured by the scanning electron microscopy (SEM; Supporting Information, Figure S3). The gravimetric current density was calculated based on the actual catalyst weight. The measured volumetric and gravimetric current densities at 0.8 V was 20.2 A cm⁻³ and 39.4 A g⁻¹, respectively. Figure 3b shows an *iR*-uncorrected polarization and power density of a similar MEA using PFeTTPP-1000 as the cathode

catalyst and Nafion 211 membrane. An open-circuit voltage (OCV) of 0.9 V was observed and the current density reached as high as 3 A cm^{-2} at 0.15 V. A peak power density of 730 mW cm^{-2} (at 0.4 V) was achieved. The cell performances observed in these tests are among the best reported recently.^[4j] The catalyst and MEA durability were also studied at both RRDE and single-cell levels. Relative fast decay on the cell voltage was found during a 100-hour test under humidified O_2 , indicating more improvement on durability is needed (see the Supporting Information).

Several characterization studies were carried out to correlate the significantly improved catalyst performance and its structure. Thermal gravimetric analysis (TGA) identified PFeTTPP weight loss at different pyrolysis temperatures during conversion of polymer into carbon. The nitrogen adsorption isotherm at 77 K was applied to study the surface area and the pore-size distribution of the samples before and after pyrolysis. Figure 4a shows two representative isotherms of PFeTTPP and PFeTTPP-700, and the incremental surface areas as the function of pore dimension calculated by NLDFT model (Figure 4b). The untreated PFeTTPP has a very high surface area (BET specific surface area or SSA = $2303 \text{ m}^2 \text{ g}^{-1}$ and Langmuir SSA = $3042 \text{ m}^2 \text{ g}^{-1}$) with pore size exclusively distributed in the micropore region ($< 2 \text{ nm}$). This surface area, to our knowledge, is the highest among the precursors used for NPMC preparation. After thermolysis, the surface area was decreased. For example, PFeTTPP-700 has BET SSA of $903 \text{ m}^2 \text{ g}^{-1}$ and Langmuir SSA of $1312 \text{ m}^2 \text{ g}^{-1}$, respectively, which are still among the highest reported values for catalyst. Even after pyrolysis at 1000°C , PFeTTPP-1000 retained a BET SSA of $758 \text{ m}^2 \text{ g}^{-1}$. Interestingly, the pore size of PFeTTPP was reduced to a lower and narrower dimension after heat-treatment (Figure 4b; Supporting Information, Figure S7). This reduction of the micropore size was quite different compared to the MOF-based precursors of which the pore dimensions were found increased after the thermolysis.^[8a,c] Such a modification can be understood from the POP molecular structure in Figure 1. As-synthesized PFeTTPP contains multiple single C–C bonds between the aromatic groups. The stacking of such bonds leads to a wider separation of the aromatic groups and thus a higher porosity. Upon thermolysis, the organic carbon in

PFeTTPP was transformed to graphitic form through elimination of single C–C bonds. Such a conversion led to the contraction of the stacking structure in Figure 1b and therefore produced a narrower pore width. High micropore distribution was identified to be favorable for ORR activity.^[4j,p]

X-ray photoelectron spectroscopy (XPS) and X-ray diffraction (XRD) were also performed to understand the chemical natures of carbon and nitrogen after thermolysis. XRD showed that pyrolyzed PFeTTPP was in the form of amorphous carbon (Supporting Information, Figure S8). C1s XPS identified several types of carbon in the spectra of PFeTTPP-700 and PFeTTPP-1000 (Supporting Information, Figure S9). The graphitic form (284 eV) was the most dominant while other types of carbons are yet to be assigned. The types of nitrogen in the carbonaceous matrix are considered more relevant to the catalyst activity.^[4p] In this study, the pyridinic and pyrrolic nitrogen were found to be the principal components by the N1s XPS in PFeTTPP-700 and PFeTTPP-1000, although the fractions of other nitrogen varied with temperature. The fractions of each type of C and N in PFeTTPP-700 and PFeTTPP-1000 were also calculated (Supporting Information, Table S1).

Elemental analysis was also carried out for the catalyst samples. The analysis found the N-content of 3.9 wt % and 1.9 wt % for PFeTTPP-700 and PFeTTPP-1000, respectively. Considering that the untreated PFeTTPP has only 4.3 wt % of nitrogen, the N-retention was relatively high during thermolysis. Although the N-content in the heat-treated PFeTTPPs are not as high as some reported NPMCs, the distinction is that the nitrogen in PFeTTPPs is highly uniform and exposed, based on the cross-linking structure of the precursor in Figure 1. Such highly dispersed N/C sites, combined with exclusive distribution of the microporosity, create a unique environment for generating a highly efficient catalyst. Another factor may have affected the catalytic activity is the presence of reasonably high level of sulfur, both in the fresh and the pyrolyzed PFeTTPPs. Sulfur was found to have a positive influence to NPMC performance.^[11] Incorporating sulfur with thiophene attached onto the POP may lead to the high S-retention during thermolysis, although more study is needed. The energy-dispersive X-ray spectroscopy (EDX)

study was also used to analyze the elemental composition of the NPMC cathode after the MEA was tested. Specific attention was paid to check if any platinum signal owing to possible cross-over from the anode; no Pt signal was found (see the Supporting Information).

In summary, we have developed a new approach to prepare highly active NPMCs for oxygen reduction for PEMFC application. A very-high-surface-

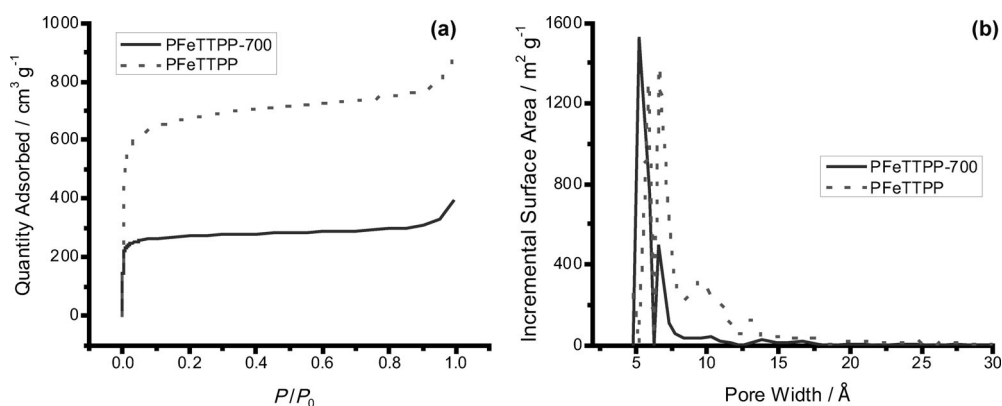


Figure 4. a) Nitrogen adsorption isotherm of fresh and heat-treated PFeTTPP; b) Pore-size distribution calculated from (a).

area POP containing uniformly distributed iron–porphyrin groups was synthesized and applied as the precursor for preparing NPMC by thermolysis. The NPMC demonstrated a high onset potential and selectivity toward the reduction of oxygen to water in the RRDE test. The MEA with such NPMC at cathode also achieved a high volumetric and gravimetric current densities and power density in the single-cell tests. Structural characterization suggested that uniformly distributed N/C sites in the micropores with high specific surface area contributed to significantly enhanced ORR activity. The reported approach shows a new route for NPMC preparation, as a variety of N-containing functional groups, serving as the ligation sites for transition metals, can be incorporated into POPs by cross-linking reactions, producing different compositions and surface properties through rational design. The POPs with various porous structures and coordination chemistry could provide more opportunities to further enhance NPMC performance and to improve the understanding on the correlation between the precursor structure and the catalytic activity.

Received: April 9, 2013

Revised: May 11, 2013

Published online: June 26, 2013

Keywords: electrocatalysis · fuel cells · oxygen reduction catalysts · polyporphyrin · porous organic polymers

- [1] a) V. Mehta, J. S. Cooper, *J. Power Sources* **2003**, *114*, 32–53; b) F. T. Wagner, B. Lakshmanan, M. F. Mathias, *J. Phys. Chem. Lett.* **2010**, *1*, 2204–2219.
- [2] a) A. J. Appleby, *J. Electroanal. Chem.* **1993**, *357*, 117–179; b) A. A. Gewirth, M. S. Thorum, *Inorg. Chem.* **2010**, *49*, 3557–3566.
- [3] H. A. Gasteiger, S. S. Kocha, B. Sompalli, F. T. Wagner, *Appl. Catal. B* **2005**, *56*, 9–35.
- [4] a) R. Bashyam, P. Zelenay, *Nature* **2006**, *443*, 63–66; b) J. Maruyama, I. Abe, *Chem. Commun.* **2007**, 2879–2881; c) T. E. Wood, Z. Tan, A. K. Schmoekel, D. O'Neill, R. Atanasoski, *J. Power Sources* **2008**, *178*, 510–516; d) C. W. B. Bezerra, L. Zhang, K. C. Lee, H. S. Liu, A. L. B. Marques, E. P. Marques, H. J. Wang, J. J. Zhang, *Electrochim. Acta* **2008**, *53*, 4937–4951; e) U. I. Koslowski, I. Abs-Wurmbach, S. Fiechter, P. Bogdanoff, *J. Phys. Chem. C* **2008**, *112*, 15356–15366; f) J. Maruyama, J. Okamura, K. Miyazaki, Y. Uchimoto, I. Abe, *J. Phys. Chem. C* **2008**, *112*, 2784–2790; g) A. Garsuch, R. d'Eon, T. Dahn, O. Klepel, R. R. Garsuch, J. R. Dahn, *J. Electrochem. Soc.* **2008**, *155*, B236–B243; h) M. Lefevre, E. Proietti, F. Jaouen, J. P. Dodelet, *Science* **2009**, *324*, 71–74; i) L. B. Wu, Y. Nabae, S. Moriya, K. Matsubayashi, N. M. Islam, S. Kuroki, M. Kakimoto, J. Ozaki, S. Miyata, *Chem. Commun.* **2010**, *46*, 6377–6379; j) F. Jaouen, E. Proietti, M. Lefevre, R. Chenitz, J. P. Dodelet, G. Wu, H. T. Chung, C. M. Johnston, P. Zelenay, *Energy Environ. Sci.* **2011**, *4*, 114–130; k) Z. W. Chen, D. Higgins, A. P. Yu, L. Zhang, J. J. Zhang, *Energy Environ. Sci.* **2011**, *4*, 3167–3192; l) G. Wu, K. L. More, C. M. Johnston, P. Zelenay, *Science* **2011**, *332*, 443–447; m) S. T. Chang, H. C. Hsu, H. C. Huang, C. H. Wang, H. Y. Du, L. C. Chen, J. F. Lee, K. H. Chen, *Int. J. Hydrogen Energy* **2012**, *37*, 13755–13762; n) M. S. Thorum, J. Yadav, A. A. Gewirth, *Angew. Chem.* **2009**, *121*, 171–173; *Angew. Chem. Int. Ed.* **2009**, *48*, 165–167; o) A. Serov, M. H. Robson, B. Halevi, K. Artyushkova, P. Atanassov, *Electrochem. Commun.* **2012**, *22*, 53–56; p) F. Jaouen, J. Herranz, M. Lefevre, J. P. Dodelet, U. I. Kramm, I. Herrmann, P. Bogdanoff, J. Maruyama, T. Nagaoka, A. Garsuch, J. R. Dahn, T. Olson, S. Pylypenko, P. Atanassov, E. A. Ustinov, *ACS Appl. Mater. Interfaces* **2009**, *1*, 1623–1639; q) D. H. Deng, L. Yu, X. Q. Chen, G. X. Wang, L. Jin, X. L. Pan, J. Deng, G. Q. Sun, X. H. Bao, *Angew. Chem.* **2013**, *125*, 389–393; *Angew. Chem. Int. Ed.* **2013**, *52*, 371–375; r) J. B. Yang, D. J. Liu, N. N. Kariuki, L. X. Chen, *Chem. Commun.* **2008**, 329–331; s) Y. G. Li, W. Zhou, H. L. Wang, L. M. Xie, Y. Y. Liang, F. Wei, J. C. Idrobo, S. J. Pennycook, H. J. Dai, *Nat. Nanotechnol.* **2012**, *7*, 394–400.
- [5] a) K. P. Gong, F. Du, Z. H. Xia, M. Durstock, L. M. Dai, *Science* **2009**, *323*, 760–764; b) S. J. Guo, S. Zhang, L. H. Wu, S. H. Sun, *Angew. Chem.* **2012**, *124*, 11940–11943; *Angew. Chem. Int. Ed.* **2012**, *51*, 11770–11773; c) J. S. Lee, G. S. Park, S. T. Kim, M. L. Liu, J. Cho, *Angew. Chem.* **2013**, *125*, 1060–1064; *Angew. Chem. Int. Ed.* **2013**, *52*, 1026–1030; d) Z. H. Wen, S. Q. Ci, F. Zhang, X. L. Feng, S. M. Cui, S. Mao, S. L. Luo, Z. He, J. H. Chen, *Adv. Mater.* **2012**, *24*, 1399–1404.
- [6] a) F. Charreter, F. Jaouen, S. Ruggeri, J. P. Dodelet, *Electrochim. Acta* **2008**, *53*, 2925–2938; b) U. I. Kramm, J. Herranz, N. Larouche, T. M. Arruda, M. Lefevre, F. Jaouen, P. Bogdanoff, S. Fiechter, I. Abs-Wurmbach, S. Mukerjee, J. P. Dodelet, *Phys. Chem. Chem. Phys.* **2012**, *14*, 11673–11688; c) M. Ferrandon, A. J. Kropf, D. J. Myers, K. Artyushkova, U. Kramm, P. Bogdanoff, G. Wu, C. M. Johnston, P. Zelenay, *J. Phys. Chem. C* **2012**, *116*, 16001–16013.
- [7] I. Herrmann, U. I. Kramm, S. Fiechter, P. Bogdanoff, *Electrochim. Acta* **2009**, *54*, 4275–4287.
- [8] a) S. Q. Ma, G. A. Goenaga, A. V. Call, D. J. Liu, *Chem. Eur. J.* **2011**, *17*, 2063–2067; b) E. Proietti, F. Jaouen, M. Lefevre, N. Larouche, J. Tian, J. Herranz, J. P. Dodelet, *Nat. Commun.* **2011**, *2*, 416; c) D. Zhao, J. L. Shui, C. Chen, X. Q. Chen, B. M. Repogle, D. P. Wang, D. J. Liu, *Chem. Sci.* **2012**, *3*, 3200–3205.
- [9] a) J. R. Holst, A. Trewin, A. I. Cooper, *Nat. Chem.* **2010**, *2*, 915–920; b) N. B. McKeown, B. Gahnm, K. J. Msayib, P. M. Budd, C. E. Tattershall, K. Mahmood, S. Tan, D. Book, H. W. Langmi, A. Walton, *Angew. Chem.* **2006**, *118*, 1836–1839; *Angew. Chem. Int. Ed.* **2006**, *45*, 1804–1807; c) J. B. Xia, S. W. Yuan, Z. Wang, S. Kirklin, B. Dorney, D. J. Liu, L. P. Yu, *Macromolecules* **2010**, *43*, 3325–3330; d) S. W. Yuan, B. Dorney, D. White, S. Kirklin, P. Zapol, L. P. Yu, D. J. Liu, *Chem. Commun.* **2010**, *46*, 4547–4549.
- [10] R. Jasinski, *Nature* **1964**, *201*, 1212–1213.
- [11] I. Herrmann, U. I. Kramm, J. Radnik, S. Fiechter, P. Bogdanoff, *J. Electrochem. Soc.* **2009**, *156*, B1283–B1292.